Chemistry–A European Journal
Research Article
doi.org/10.1002/chem.202402454
Chemistry Europe
European Chemical Societies Publishing
www.chemeurj.org

Hot Paper

Changes in Secondary Structure Upon Pr to Pfr Transition in Cyanobacterial Phytochrome Cph1 Detected by DNP NMR

Lisa Gerland,*[a] Anne Diehl,[a] Natalja Erdmann,[a] Matthias Hiller,[a] Christina Lang,[b] Christian Teutloff,[c] Jon Hughes,[b, c] and Hartmut Oschkinat*[a]

Phytochromes perceive subtle changes in the light environment and convert them into biological signals by photoconversion between the red-light absorbing (Pr) and the far-red-absorbing (Pfr) states. In the primitive bacteriophytochromes this includes refolding of a tongue-like hairpin loop close to the chromophore, one strand of an antiparallel β-sheet being replaced by an α-helix. However, the strand sequence in the cyanobacterial phytochrome Cph1 is different from that of previously investigated bacteriophytochromes and has a higher β-sheet propensity. We confirm here the transition experimentally and estimate minimum helix length using dynamic nuclear polarisation (DNP) magic angle spinning NMR. Sample conditions were optimized for protein DNP NMR studies at high field, yielding Boltzmann enhancements ε_B of 19 at an NMR field of 18.801 T. Selective labelling of Trp, Ile, Arg, and Val residues with ^{13}C and ^{15}N enabled filtering for pairs of labelled amino acids by the 3D CANCOCA technique to identify signals of the motif $_{483}$Ile-Val-Arg$_{485}$ (IVR) present in both sheet and helix. Those signals were assigned for the Pfr state of the protein. Based on the chemical shift pattern, we confirm for Cph1 the formation of a helix covering the IVR motif.

Introduction

Photoreceptor proteins of the phytochrome family are ubiquitous in plants and widely represented in algae, cyanobacteria and non-photosynthetic bacteria.[1,2] Whereas in plants they serve as exquisitely sensitive light detectors and in the perception of both canopy shade and daylength, prokaryotic phytochromes are involved in chromatic acclimation, phototaxis towards or away from light, cell aggregation as protective mechanism against harmful wavelengths and photomorphogenic effects.[1,2] Although the function of the Cph1 phytochrome from *Synechocystis* 6803 investigated here[3] is still unknown, it represents a valuable model for mechanistic investigations due to the greater sequence similarity of its photosensory module to that of plant phytochromes.

Phytochromes are dimeric, each protomer carrying a bilin chromophore[1,4,5] that undergoes light-induced conformational changes on a picosecond timescale[6] as the origin of the signalling process[7,8] (Figure 1A). Canonical and bathy-type phytochromes are known in which the resting state of the photocycle is either Pr or Pfr, respectively. The chromophore is located in the N-terminal photosensory module (PSM)[9] comprising Period/ARNT/single-minded (PAS),[10] cGMP-phosphodiesterase/adenylyl-cyclase/FhlA (GAF)[11] and phytochrome-specific (PHY)[12] domains (Figure 1B). The GAF domain bears the chromophore, attached covalently at a conserved cysteine residue. The PSMs of the canonical phytochromes Cph1 (Figure 1C; PDB: 2VEA),[13] *Dr*BphP from *Deinococcus radiodurans* (PDB: 4Q0J,[14] 8AVW[15]), *Xcc*BphP from *Xanthomonas campestris* (PDB:6PLK)[16] and *Is*PadC from *Idiomarina* A28 L (PDB: 5LLW)[17] show intimately associated PAS and GAF domains, whereas the PHY domain is held at a distance by a long α-helical spine and an additional, tongue-like two-stranded β-sheet structure (Figure 1C, D). The tongue seals the chromophore pocket close to chromophore ring A.[7,13] In contrast, bathy-type bacteriophytochromes in the Pfr state show a helix in place of the two-stranded sheet.[16,18–22] Initially, these structural differences were observed in canonical and bathy-type phytochromes, respectively. A β-sheet to α-helix photoconversion within the same protein is difficult to observe since a Pr/Pfr photoequilibrium rather than pure Pfr is obtained by illumination of the wild-type proteins.[8,23–25] Despite these difficulties, both states were described for the bacteriophytochromes *Dr*BphP, *Xcc*BphP and *Is*PadC by applying a combination of methods[14,16,17,26–28] whereby illuminated crystals containing both forms were investigated. For *Dr*BphP, the conversion was confirmed later by a high resolution X-ray structure of the mutant F469 W that crystalized

[a] L. Gerland, A. Diehl, N. Erdmann, M. Hiller, H. Oschkinat
NMR-supported Structural Biology, Leibniz-Forschungsinstitut für Molekulare Pharmakologie, Robert-Rössle-Str. 10, 13125 Berlin, Germany
E-mail: Oschkinat@fmp-berlin.de
Gerland@fmp-berlin.de
[b] C. Lang, J. Hughes
Plant Physiology, Faculty of Biology and Chemistry, Justus-Liebig-University Giessen, Senckenbergstr. 3, 35390 Giessen, Germany
[c] C. Teutloff, J. Hughes
Department of Physics, Freie Universität Berlin, Arnimallee 14, 14195 Berlin, Germany

Supporting information for this article is available on the WWW under https://doi.org/10.1002/chem.202402454

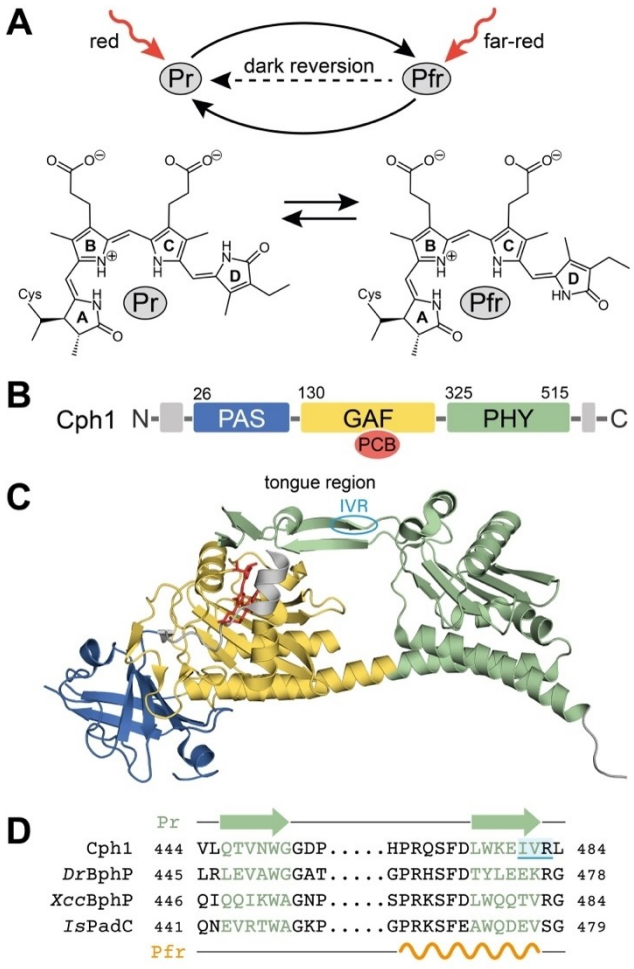

Figure 1. A Photoconversion of phytochrome, without showing intermediate states, and structures of the phycocyanobilin chromophore in Pr and Pfr states with the D ring flip. The resonance structure with the most likely position of the positive charge is indicated. B Domain composition and C 2VEA crystal structure of the Cph1△2 Pr form with PCB chromophore indicated in red. The investigated sequence segment is indicated by an ellipsoid. D Comparison of 'tongue' region sequences. Secondary structure motifs displayed for Pr in green and Pfr in orange. The IVR motif in Cph1 is highlighted.

predominantly in the Pfr state, and supported by cryo-EM investigations.[14,29] Tongue refolding was suggested to be the central event in intramolecular signalling.[,28a] In the dimer, the shorter helical (Pfr) conformation would pull the PHY domains apart and thereby potentially change the enzymatic activity of the C-terminal output module, commonly a histidine protein kinase. However, this proposal was based on studies of the isolated PSM, not the full-length dimer. Notably, pulsed electron-electron double resonance (PELDOR) measurements of the full-length dimer of Agp1 bacteriophytochrome from *Agrobacterium* failed to show the expected shifts.[28b]

The present work focuses on detecting the Pr→Pfr transition in the PSM of Cph1 (Cph1△2) by DNP NMR.[30–33] In Cph1, the strand that is expected to photoconvert from sheet to helix is divergent from its bacteriophytochrome counterparts and has reduced helical propensity on account of sheet-promoting residues such as Ile and Val (Figure 1D).[34] Thus we were interested to determine the extent of the helix in Cph1 Pfr since it would determine the proposed shortening effect on the tongue. While different phytochromes have already been investigated by solution NMR,[35–37] our Cph1△2 construct (514 residues, 59 kDa) is rather large for such methods. In this study, we thus employed magic angle spinning (MAS) NMR after sedimenting the sample by ultracentrifugation, in conjunction with DNP. In this context, we applied a protein sample preparation protocol that involves low glycerol levels. Further, we simplified the crowded PSM NMR spectra by employing amino acid-selective ^{13}C,^{15}N-labelling of Ile, Arg, and Val together with filtering of C_α-C_α correlations *via* the 3D CANCOCA technique.[38,39] This enabled us to detect the chemical shifts of the amino acid triplet IVR that is solely present in the tongue region (Figure 1D). Especially the C_α and C_β chemical shifts of amino acids are characteristically influenced by secondary structure, hence emerging Pfr signals should be readily recognizable in those 3D CANCOCA spectra. Since 7 Trp residues are present in the PSM and two of them at the edge of the double-stranded β-sheet, ^{13}C, ^{15}N-labelled Trp was also included in the labelling pattern. To support the enhancement and to avoid a loss of ^{15}N of the provided amino acids W, I, R, V, all other amino acids were ^{2}H,^{15}N-labelled, resulting in [u-^{2}H,^{15}N; W,I,R,V-^{1}H,^{13}C,^{15}N]-Cph1△2.

Experimental Section

Preparation of [u-^{2}H,^{15}N; W,I,R,V-^{1}H,^{13}C,^{15}N]-Cph1△2

The plasmid p926.5 encoding Cph1△2 (the N-terminal NTS-PAS-GAF and PHY domains of Cph1, residues 1–514 with a C-terminal 6xHis tag) was co-transformed with pSE111 encoding for $lacI^q$ and ArgU into *E.coli* BL21 (DE3) cells using a standard heat shock protocol. A 400 ml pre-culture was grown overnight at 30 °C, 170 rpm in LB medium containing kanamycin (40 μg x mL^{-1}) and carbenicillin (60 μg x mL^{-1}). Cells were spun down (RT, 10 min, 2000 g), resuspended in 2 L 2x M9 medium (D_2O, D12-glucose, ^{15}N-NH_4Cl) and grown for 5 h at 37 °C, 170 rpm before addition of a ^{15}N,^{13}C-labelled mix of arginine, isoleucine, tryptophan and valine (30 mg each) in D_2O. After 1 h at 18 °C, 160 rpm, protein expression was induced with 100 μM IPTG. The consumption of nutrients was detected by measuring glucose and ammonium chloride levels using sensory strips (Merck Ammonium and Glucose Test). Both nutrients were added when one was detected below a level of 10 mg x l^{-1}. Accordingly, 2 g x l^{-1} D_{12}-glucose, 0.5 g x l^{-1} ^{15}N-NH_4Cl and 25 mg x l^{-1} of each ^{15}N,^{13}C-labelled arginine, isoleucine, tryptophan, and valine were applied after expression for 17 h. After further 6 h 1 g x l^{-1} D_{12}-glucose, 0.25 g x l^{-1} ^{15}N-NH_4Cl and 60 mg x l^{-1} pro ^{15}N,^{13}C-labelled arginine, isoleucine, tryptophan, and valine were added. In the end, 115 mg x l^{-1} of each of the 4 amino acids were applied. After growth for 42 h at 18 °C, cells were harvested at 4000 g, washed in 150 mM NaCl and stored at −80 °C. The purified and uniformly ^{2}H, ^{15}N labelled Cph1△2 sample with arginine, isoleucine, tryptophan and valine ^{1}H,^{13}C, ^{15}N labelled ([u-^{2}H,^{15}N; W,I,R,V-^{1}H,^{13}C,^{15}N]-Cph1△2) was assembled with unlabeled phycocyanobilin (isotopes in natural abundance) according to Jaedicke et al.[40]

Standard Radical Samples with Proline as Readout

A 0.5 M stock solution of ^{15}N,^{13}C proline in 60% glycerol, 30% D_2O and 10% H_2O (hereafter referred to as "GDH") was prepared. M-TinyPol[41] and bcTol-M[42] were dissolved in GDH at 20 mM concentration. To fully dissolve, M-TinyPol was subjected to sonication for 10 minutes. In order to prepare a radical-free sample for comparison, the proline stock solution and GDH buffer were mixed in a 1:1 ratio, and 10 µl of this mixture were pipetted into a 1.9 mm rotor. For the radical containing samples, the bcTol-M or M-Tinypol solutions were mixed 1:1 with the proline stock solution. The final concentration of bcTol-M or M-TinyPol was 10 mM, and the proline concentration was 0.25 M. From these solutions, 10 µl were filled into each rotor. With this procedure it is ensured that all rotors contain the same amount of proline. The rotors were stored at −20 °C before and after NMR measurements.

Preparation of Pr and Pr/Pfr-State Cph1△2 Samples

Cph1△2 was irradiated at 730 or 660 nm for 1.5 h on ice, to generate Pr or mixed Pr/Pfr states, respectively. The photoconversion was monitored by UV-Vis spectroscopy. 15 mg of Cph1△2 in 50 mM $NaPO_4$ buffer (pH 7.8, 20% D_2O) were filled into a 1.9 mm rotor via ultracentrifugation for 62–68 h at 71000 g at 4 °C. 40 mM bcTol-M and M-TinyPol stock solutions in GDH were prepared whereby the M-TinyPol solution was sonicated for 20 minutes. 2.2 µl of the respective radical solution were added to each of the ultra-centrifuged [u-^{2}H,^{15}N; W,I,R,V-^{1}H,^{13}C,^{15}N]-Cph1△2 rotors, leading to a final radical concentration of 10 mM and ~10% glycerol for both rotors. Pr state Cph1△2 was kept in the dark and stored at 20 °C, Pr/Pfr Cph1△2 was irradiated at 660 nm prior to closure of the rotor, after which the rotor was immediately plunge-frozen in liquid nitrogen to prevent dark reversion.

Characterization of Standard Radical Samples

One-dimensional hC-CP spectra were recorded with an acquisition time of 5.1 ms, 4 dummy scans and 1024 complex points. The CP contact time was 2 ms for both samples. The amplitude of the ^{1}H spin-lock pulse was ramped from ~59 to ~74 kHz and the ^{13}C spin-lock rf-field was kept constant at 37 kHz and 43 kHz for the bcTol-M and M-TinyPol samples, respectively. Spinal64 heteronuclear decoupling was employed during acquisition with a nominal B_0-field of 78 kHz. All spectra were processed using the same window function (EM, LB = 100 Hz). To compare the enhancement and thus efficiency of both radicals, hC-CP spectra were recorded with and without microwave irradiation. After correcting for the number of scans, the enhancements and reduced Boltzmann enhancements were calculated with the following equations:

$$\varepsilon = \frac{I_{on}}{I_{off}} \text{ and } \varepsilon_B = \frac{I_{on}}{I_{off}}\varepsilon_{depo}.$$

The depolarization factor ε_{depo} takes into account the depolarization and quenching effects characteristic for the employed polarizing agents. It is 0.5 for bcTol-M[43] and 0.65 for M-TinyPol.[41]

DNP NMR – Recording of [u-^{2}H,^{15}N; W,I,R,V-^{1}H,^{13}C,^{15}N]-Cph1△2 Pr and Pr/Pfr Spectra

3D CANCOCA spectra were recorded with 16 scans, 16 dummy scans and 512x48x96 data points. Acquisition times were 6 ms in F1 (^{13}C), 7.2 ms in F2 (^{15}N) and 8.3 ms in F3 (^{13}C), the respective spectral widths were 8000 Hz (F1), 3333 Hz (F2) and 61729 Hz (F3). The pulse sequence can be found in Shi et al.[39] All parameters used for recording the spectra of the two different samples, Pr and Pr/Pfr Cph1△2, can be found in Table S1. 3D hNCACB spectra were recorded with 8 dummy scans, 16 scans and 1024x72x64 data points. Acquisition times were 17.2 ms in F1 (^{13}C), 3.6 ms in F2 (^{13}C) and 12.8 ms in F3 (^{15}N). The respective spectral widths were 2500 Hz (F1), 10000 Hz (F2) and 59524 Hz (F3). For the initial hN CP, a constant ^{1}H rf-field of 64 kHz for Pr and 69 kHz for Pr/Pfr was applied, whereas the rf-field on ^{15}N was ramped from 46 to 51 kHz for Pr and from 49 to 55 kHz for Pr/Pfr. The hN CP contact time was 400 µs for Pr and 600 µs for Pr/Pfr. The NCA SPECIFIC CP[44] contact time was 5500 µs for Pr (7000 µs for Pr/Pfr), with a constant rf-field of 48 kHz on ^{15}N for Pr (51 kHz for Pr/Pfr) and a ramped ^{13}C rf-field from 22 to 31 kHz for both the Pr and Pr/Pfr sample. The DREAM[45] transfer contact time was 1.8 ms for both samples. The hNCA spectrum and the ^{13}C-^{13}C DARR correlation (20 ms mixing) were recorded with the same or similar parameters.

Results and Discussion

Performance of Radicals at 800 MHz

As a first step, we benchmarked the DNP efficiency of two radicals at an 800 MHz ^{1}H NMR frequency spectrometer equipped with a commercial gyrotron and a probe for 1.9 mm rotors, since measurements at this high field and rotor size are not yet routine. Field profiles of the radicals M-TinyPol[41] and bcTol-M[42] were recorded on standard proline samples (Figure S1), covering a narrow B_0 range from 18.805 to 18.787 Tesla within which maximum enhancement was expected. bcTol-M and M-TinyPol show ^{13}C Boltzmann enhancements (ε_B) of 44 and 42 on proline carbon signals at 18.801 T, respectively. Protocols for preparing DNP samples typically employ high amounts of glycerol to avoid the formation of ice crystals and as a result regions of high radical concentration with increased electron relaxation. Such effects lead to a reduction of enhancement.[33,46–48] In an attempt to minimize the glycerol concentration and effectively use more volume for the analyte in the limited space of the NMR rotor, we sedimented the dissolved protein into a 1.9 mm rotor at 71000 *g*, and added radical dissolved in d_8-glycerol such that the final glycerol concentration was 10–15%. In this way, a very concentrated protein gel is formed with a low tendency to form ice crystals. However, under these conditions, the phytochrome sample containing M-TinyPol lost enhancement between measurements, which we attribute to low solubility in low glycerol buffer. We thus continued with the bcTol-M sample. To confirm the suitability of the low glycerol buffer further, we investigated the bcTol-M EPR spectrum of our low-glycerol, sedimented Cph1△2 sample by CW EPR saturation experiments at 9.4 GHz and compared it to the saturation of bcTol-M EPR signals in proline standard samples with 60% glycerol. Indeed, both matrices have a similar influence on the bcTol-M radical. The half-saturation microwave strengths $P_{1/2}$ are very similar for both preparations, approximately 1 mW at 100 K and 3.5 mW at 200 K (Figure S2). These findings strongly imply comparable electron spin relaxation times in both samples, explaining the substantial DNP enhancement observed on our protein sample.

At 18.801 T NMR field, ε_B of the bcTol-M containing protein sample was 19.0 (Figure S3) and thus still more than 40% of the ε_B observed on the proline samples that contained 60% glycerol.

Light-Induced Structural Changes in Cph1△2

A 2D ^{13}C-^{13}C correlation of [u-^{2}H,^{15}N; W,I,R,V-^{1}H,^{13}C,^{15}N]-Cph1△2 was recorded for initial characterization Figure S4). As expected from the size of the protein, the spectrum shows considerable signal overlap. For orientation, spectral regions with cross peaks typical for the labelled amino acids are indicated in the expansions to the right in Figure S4. Experience shows that signals from amino acids on the surface show multiple signals since conformations are frozen out at 100 K, whereas residues in the core are likely locked in one conformation and therefore show only one dominant signal.

3D NCACX[50] and 3D CANCOCA spectra of [u-^{2}H,^{15}N; W,I,R,V-^{1}H,^{13}C,^{15}N]-Cph1△2 were recorded on dark and illuminated samples. Photoconversion was carried out prior to rotor filling in darkness and the material immediately freeze-trapped afterwards. UV/Vis spectra indicated a ca. 1:2 mix of Pr and Pfr states, thus CANCOCA spectra are expected to include Pr signals. Taking advantage of the Trp, Ile, Val, Arg labelling pattern, 3D CANCOCA spectra of Cph1△2 in each of the Pr and Pfr states are expected to show only 21 peaks and thus reduced overlap in the 3D spectrum. An impression of the selectivity imposed by this strategy is apparent from Figure S5 that shows a 2D projection of the 3D CANCOCA (red) over a hNCA correlation (blue). Still, signals are broad and it is likely that multiple signals appear for some sites, i.e. pairs of amino acids. In Figure 2, two ^{13}C-^{13}C planes of 3D CANCOCA spectra from samples containing either pure Pr (blue) or mixed Pr/Pfr (red) are shown. The C_α-C_α cross peak labelled 'VR-pair' is exclusively present in the Cph1△2 Pfr spectrum, the same holds for the 'IV-pair' labeled cross peak. In addition, planes from the Pr/Pfr 3D NCACB spectrum (black) are shown, extracted at the same nitrogen frequencies as indicated at the bottom right. The schemes below the spectra illustrate the magnetisation transfer in the CANCOCA experiment leading to the cross peaks for the VR-pair (left) and the IV-pair (right). The two peaks originate from a sequential triplet, as they share the C_α resonance at 64.7 ppm indicated by the red lines connecting the two signals. The central residue of the triplet is assigned to a valine by means of the C_β chemical shift. Whilst the C_α chemical shifts of Ile and Val are similar, their C_β resonances differ, with average shifts of 38.6 ppm and 32.7 ppm, respectively (see Figure 3). Since the residue subsequent to the valine has C_α chemical shifts characteristic for an arginine, these signals can thus be assigned either to a VVR- or an IVR-triplet. To distinguish between the two possibilities, we exploit the fact that only one IVR triplet is present in the protein sequence and no VVR-triplet. Hence, the two peaks can be unambiguously assigned to the IVR motif of the tongue. The ^{15}N chemical shifts of the arginine and valine are shown in the left and right pannels of Figure 2, respectively. As the signals of the three residues only occur after illumination and show chemical shifts typical for residues in an α-helical configuration, we conclude that the tongue forms an α-helix in the Pfr state. This helix is at least as extensive as that observed in bacteriophytochromes, indeed the subsequent arginine residue also shows a Cα-chemical shift typical of a helix.

It was not possible to assign the IVR-triplet in the Pr state of Cph1△2. The expected pattern with ^{13}C chemical shifts of β-sheet residues is either hidden by overlapping peaks in the bulk, or heterogenously broadened due to disorder, as suggested by Gustavsson et al.[37] Structural disorder in this region in the Pr state is not unlikely, since when performing solution NMR experiments on the bacteriophytochrome *Dr*BphP, it was not possible to assign backbone resonances for the tongue in the dark-adapted Pr state.[37] Switching from a disordered to a more homogenously structured state is a common event in signalling processes.

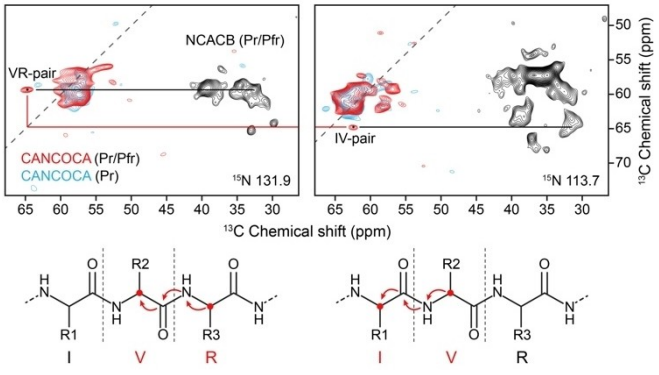

Figure 2. Detection of C_α - C_α cross peaks of the IVR-triplet in the Pfr state. 800 MHz DNP NMR spectra of Pr and Pr/Pfr [u-^{2}H,^{15}N; W,I,R,V-^{1}H,^{13}C,^{15}N]-Cph1△2 recorded at 20 kHz MAS, 105 K. Superposition of ^{13}C-^{13}C slices extracted at different ^{15}N frequencies from CANCOCA spectra of [u-^{2}H,^{15}N; W,I,R,V-^{1}H,^{13}C,^{15}N]-Cph1△2 in Pr (blue) and Pr/Pfr state (red) with the Pr/Pfr state NCACB spectrum in black. 'VR-pair' in the left top panel indicates the correlation of arginine C_α with valine C_α. 'IV-pair' in the top right panel indicates the C_α-C_α correlation of a valine and an isoleucine residue. The corresponding magnetisation transfers are indicated by arrows in the drawings at the bottom, for the VR-pair (left) and the IV-pair (right).

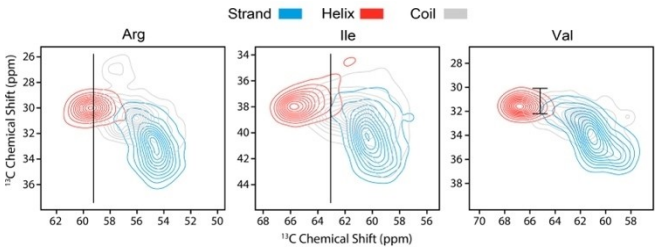

Figure 3. Distribution of C_α and C_β resonances of the indicated amino acids depending on secondary structure. The PACSY NMR chemical shift database was implemented to generate the 2D plots.[49] The lines indicate the C_α chemical shift of the respective residue in the Pfr form IVR motif as observed in the CANCOCA spectrum, C_β is unknown. For the valine residue the NCACB spectrum provides information about the position of the C_β shift, hence the better-defined area.

Conclusions

We have provided evidence for the sheet to helix transition in the tongue region of the cyanobacterial phytochrome Cph1 upon Pr→Pfr photoconversion. We thus show that the resulting helix in Pfr is at least as long as in the previously investigated bacteriophytochrome examples, *Dr*BphP, *Xcc*BphP, and *Is*PadC, despite considerable sequence divergence (Figure 1D). Indeed, the sheet sequence in Cph1△2 ($_{479}$LWKEIV$_{484}$) has a higher β-sheet propensity due to the IV-pair than in *Dr*BphP ($_{486}$TYLEEK$_{491}$). The chemical shift of the R483 C_α signal indicates that the helix in Cph1 Pfr even includes R483.

By applying DNP solid state NMR, we show that it is possible to analyse structural transitions in phytochromes upon light irradiation in a single sample. This technique has been shown to be valuable for investigating light-driven conformational transitions.[51,52] DNP NMR requires cryogenic temperatures that are beneficial when working with phytochrome solutions since thermal Pr/Pfr reversion is slow on the time scale of measurement. To obtain the required sequence-specific assignments of this large protein (on the NMR scale), it was critical to apply an NMR technique that yields correlations between adjacent C_α nuclei to filter for pairs of the ^{13}C, ^{15}N- labelled amino acids Trp, Ile, Arg, and Val. In combination with such amino acid-selective ^{13}C, ^{15}N-labelling, DNP enhancement allows application of a relatively insensitive technique, 3D CANCOCA, that filters for pairs of ^{13}C, ^{15}N-labelled residues. The required signal-to-noise ratio was achieved by DNP, while new sample preparation methods were applied that may be considered general for the investigation of proteins. We worked with a highly concentrated protein gel generated by ultracentrifugation; hence the probability of ice crystal formation *and* sample degradation is reduced even without large amounts of glycerol in the sample. A similar approach has been applied earlier to sedimented proteins[53] and in studies on membranes[52] as well as whole cell systems.[54] Through the experiments described here we were able to confirm the helical conformation of the tongue in the cyanobacterial phytochrome Cph1, and determined the helix length to include the IVR motif.

Supporting Information Summary

The authors have cited additional references within the Supporting Information.[55]

Acknowledgements

This work was supported by the Deutsche Forschungsgemeinschaft, SFB 1078 (H.O. and J.H). The authors are grateful to Dr. Olivier Ouari, Marseille, and Dr. Snorri Sigurdsson, Reikjavik, for providing the radicals M-TinyPol and bcTol-M, respectively. The authors thank further Dr. Barth van Rossum for comments on the manuscript and the preparation of figures, and Dr. Miguel Arbesu for his support regarding Figure 3. Open Access funding enabled and organized by Projekt DEAL.

Conflict of Interests

The authors declare no conflict of interest.

Data Availability Statement

The data that support the findings of this study are available from the corresponding author upon reasonable request.

Keywords: NMR spectroscopy · Phytochrome · Dynamic nuclear polarization · Chromophore · Secondary structure

[1] J. Hughes, A. Winkler, *Ann. Rev. Plant. Biol.* **2024**, *75*, 153–183.
[2] L. B. Wiltbank, D. M. Kehoe, *Nat. Rev. Microbiol.* **2019**, *17*, 37–50.
[3] T. Lamparter, B. Esteban, J. Hughes, *Eur. J. Biochem.* **2001**, *268*, 4720–4730.
[4] C. Bongards, W. Gärtner, *Acc. Chem. Res.* **2010**, *43*, 485–495.
[5] F. V. Escobar, D. von Stetten, M. Günther-Lütkens, A. Keidel, N. Michael, T. Lamparter, L. O. Essen, J. Hughes, W. Gärtner, Y. Yang, K. Heyne, M. A. Mroginski, P. Hildebrandt, *Front. Mol. Biosci.* **2015**, *2*, 1–13.
[6] E. Claesson, W. Y. Wahlgren, H. Takala, S. Pandey, L. Castillon, V. Kuznetsova, L. Henry, M. Panman, M. Carrillo, J. Kübel, R. Nanekar, L. Isaksson, A. Nimmrich, A. Cellini, D. Morozov, M. Maj, M. Kurttila, R. Bosman, E. Nango, R. Tanaka, T. Tanaka, L. Fangjia, S. Iwata, S. Owada, K. Moffat, G. Groenhof, E. A. Stojković, J. A. Ihalainen, M. Schmidt, S. Westenhoff, *eLife* **2020**, *9*, 1–18.
[7] A. T. Ulijasz, G. Cornilescu, C. C. Cornilescu, J. Zhang, J. L. Markley, R. D. Vierstra, *Nature* **2010**, *463*, 250–254.
[8] N. C. Rockwell, Y. S. Su, J. C. Lagarias, *Annu. Rev. Plant Biol.* **2006**, *57*, 837–858.
[9] S. Von Horsten, S. Straß, N. Hellwig, V. Gruth, R. Klasen, A. Mielcarek, U. Linne, N. Morgner, L. O. Essen, *Sci. Rep.* **2016**, *6*, 1–8.
[10] A. Möglich, R. A. Ayers, K. Moffat, *Structure* **2009**, *10*, 1282–1294.
[11] Y. S. J. Ho, L. M. Burden, J. H. Hurley, *EMBO J.* **2000**, *19*, 5288–5299.
[12] N. C. Rockwell, J. C. Lagarias, *Plant Cell* **2006**, *18*, 4–14.
[13] L. O. Essen, J. Mailliet, J. Hughes, *PNAS* **2008**, *105*, 14709–14714.
[14] E. S. Burgie, T. Wang, A. N. Bussell, J. M. Walker, H. Li, R. D. Vierstra, *J. Biol. Chem.* **2014**, *289*, 24573–24587.
[15] W. Y. Wahlgren, E. Claesson, I. Tuure, S. Trillo-Muyo, S. Bódizs, J. A. Ihalainen, H. Takala, S. Westenhoff, *Nat. Commun.* **2022**, *13*, 1–8.
[16] L. H. Otero, S. Foscaldi, G. T. Antelo, G. L. Rosano, S. Sirigu, S. Klinke, L. A. Defelipe, M. Sánchez-Lamas, G. Battocchio, V. Conforte, A. A. Vojnov, L. M. G. Chavas, F. A. Goldbaum, M. A. Mroginski, J. Rinaldi, H. R. Bonomi, *Sci. Adv.* **2021**, *7*, 1–22.
[17] G. Gourinchas, S. Etzl, C. Göbl, U. Vide, T. Madl, A. Winkler, *Sci. Adv.* **2017**, *3*, 3.
[18] X. Yang, Z. Ren, J. Kuk, K. Moffat, *Nature* **2011**, *479*, 428–431.
[19] F. Velazquez Escobar, P. Piwowarski, J. Salewski, N. Michael, M. Fernandez Lopez, A. Rupp, B. M. Qureshi, P. Scheerer, F. Bartl, N. Frankenberg-Dinkel, F. Siebert, M. Andrea Mroginski, P. Hildebrandt, *Nat. Chem.* **2015**, *7*, 423–430.
[20] A. Schmidt, L. Sauthof, M. Szczepek, M. F. Lopez, F. V. Escobar, B. M. Qureshi, N. Michael, D. Buhrke, T. Stevens, D. Kwiatkowski, D. von Stetten, M. A. Mroginski, N. Krauß, T. Lamparter, P. Hildebrandt, P. Scheerer, *Nat. Commun.* **2018**, *9*, 1–13.
[21] X. Yang, J. Kuk, K. Moffat, *PNAS* **2008**, *105*, 14715–14720.
[22] X. Yang, J. Kuk, K. Moffat, *Proc. Natl. Acad. Sci. USA* **2009**, *106*, 15639–15644.
[23] A. Rivadossi, F. M. Garlaschi, A. P. Casazza, G. Zucchelli, R. C. Jennings, *Photochem. Photobiol. Sci.* **2008**, *7*, 986–990.
[24] C. Klose, F. Nagy, E. Schäfer, *Mol. Plant Pathol.* **2020**, *13*, 386–397.
[25] K. C. Yeh, J. C. Lagarias, *Proc. Natl. Acad. Sci. USA* **1998**, *95*, 13976–13981.
[26] G. Gourinchas, U. Heintz, A. Winkler, *eLife* **2018**, *7*, 1–25.
[27] L. H. Otero, S. Klinke, J. Rinaldi, F. Velázquez-Escobar, M. A. Mroginski, M. Fernández López, F. Malamud, A. A. Vojnov, P. Hildebrandt, F. A. Goldbaum, H. R. Bonomi, *J. Mol. Biol.* **2016**, *428*, 3702–3720.
[28] a) H. Takala, A. Björling, O. Berntsson, H. Lehtivuori, S. Niebling, M. Hoernke, I. Kosheleva, R. Henning, A. Menzel, J. A. Ihalainen, S. Westenhoff, *Nature* **2014**, *509*, 245–248; b) K. Anders, G. Daminelli-Widany, M. A.

Mroginski, D. von Stetten, L.-O. Essen, *J. Biol. Chem.* **2013**, *288*, 35714–25; c) S. Kacprzak, I. Njimona, A. Renz, J. Feng, E. Reijerse, W. Lubitz, N. Krauss, P. Scheerer, S. Nagano, T. Lamparter, S. Weber, *J. Biol. Chem.* **2017**, *292*, 7598–7606.
[29] E. S. Burgie, J. Zhang, R. D. Vierstra, *Structure* **2016**, *24*, 448–457.
[30] A. B. Barnes, G. De Paëpe, P. C. A. Van Der Wel, K. N. Hu, C. G. Joo, V. S. Bajaj, M. L. Mak-Jurkauskas, J. R. Sirigiri, J. Herzfeld, R. J. Temkin, R. G. Griffin, *Appl. Magn. Reson.* **2008**, *34*, 237–263.
[31] T. Maly, G. T. Debelouchin, S. B. Vikram, K.-N. Hu, C. G. Joo, M. L. Mak-Jurkauskas, J. R. Sirigiri, P. C. A. Van Der Wel, J. Herzfeld, R. J. Temkin, R. G. Griffin, *J. Chem. Phys.* **2008**, *128*.
[32] J. H. Ardenkjaer-Larsen, G. S. Boebinger, A. Comment, S. Duckett, A. S. Edison, F. Engelke, C. Griesinger, R. G. Griffin, C. Hilty, H. Maeda, G. Parigi, T. Prisner, E. Ravera, J. Van Bentum, S. Vega, A. Webb, C. Luchinat, H. Schwalbe, L. Frydman, *Angew. Chem. Int. Ed.* **2015**, *54*, 9162–9185.
[33] D. A. Hall, D. C. Maus, G. J. Gerfen, S. J. Inati, L. R. Becerra, F. W. Dahlquist, R. G. Griffin, *Science* **1997**, *276*, 930–932.
[34] S. N. Malkov, M. V. Živković, M. V. Beljanski, M. B. Hall, S. D. Zarić, *J. Mol. Model.* **2008**, *14*, 769–775.
[35] H. M. Strauss, J. Hughes, P. Schmieder, *Biochemistry* **2005**, *44*, 8244–8250.
[36] L. Isaksson, E. Gustavsson, C. Persson, U. Brath, L. Vrhovac, G. Karlsson, V. Orekhov, S. Westenhoff, *Structure* **2021**, *29*, 151–160.
[37] E. Gustavsson, L. Isaksson, C. Persson, M. Mayzel, U. Brath, L. Vrhovac, J. A. Ihalainen, B. G. Karlsson, V. Orekhov, S. Westenhoff, *Biophys. J.* **2020**, *118*, 415–421.
[38] V. Chevelkov, C. Shi, H. K. Fasshuber, S. Becker, A. Lange, *J. Biomol. NMR* **2013**, *56*, 303–311.
[39] C. Shi, H. K. Fasshuber, V. Chevelkov, S. Xiang, B. Habenstein, S. K. Vasa, S. Becker, A. Lange, *J. Biomol. NMR* **2014**, *59*, 15–22.
[40] K. Jaedicke, A. L. Lichtenthäler, J. Hughes, *Proc. Natl. Acad. Sci. USA* **2012**, *109*(30), 12231–12236.
[41] A. Lund, G. Casano, G. Menzildjian, M. Kaushik, G. Stevanato, M. Yulikov, R. Jabbour, D. Wisser, M. Renom-Carrasco, C. Thieuleux, F. Bernada, H. Karoui, D. Siri, M. Rosay, I. V. Sergeyev, D. Gajan, M. Lelli, L. Emsley, O. Ouari, A. Lesage, *Chem. Sci.* **2020**, *11*, 2810–2818.
[42] A. P. Jagtap, M. A. Geiger, D. Stöppler, M. Orwick-Rydmark, H. Oschkinat, S. T. Sigurdsson, *Chem. Commun.* **2016**, *52*, 7020–7023.
[43] F. Mentink-Vigier, T. Dubroca, J. Van Tol, S. T. Sigurdsson, *J. Magn. Reson.* **2021**, *329*, 107026.
[44] M. Baldus, A. T. Petkova, J. Herzfeld, R. G. Griffin, *Mol. Phys.* **1998**, *95*, 1197–1207.
[45] R. Verel, M. Ernst, B. H. Meier, *J. Magn. Reson.* **2001**, *150*, 81–99.
[46] M. Rosay, V. Weis, K. E. Kreischer, R. J. Temkin, R. G. Griffin, *J. Am. Chem. Soc.* **2002**, *124*, 3214–3215.
[47] E. P. Kirilina, I. A. Grigoriev, S. A. Dzuba, *J. Chem. Phys.* **2004**, *121*, 12465–12471.
[48] E. R. Georgieva, A. S. Roy, V. M. Grigoryants, P. P. Borbat, K. A. Earle, C. P. Scholes, J. H. Freed, *J. Magn. Reson.* **2012**, *216*, 69–77.
[49] Woonghee Lee, W. Yu, S. Kim, I. Chang, Weontae Lee, J. L. Markley, *J. Biomol. NMR* **2012**, *54*, 169–179..
[50] J. Pauli, M. Baldus, B. J. Van Rossum, H. De Groot, H. Oschkinat, *ChemBioChem* **2001**, *2*(4), 272–281.
[51] J. Becker-Baldus, A. Leeder, L. J. Brown, R. C. D. Brown, C. Bamann, C. Glaubitz, *Angew. Chem. Int. Ed.* **2021**, *60*, 16442–16447.
[52] J. Becker-Baldus, C. Glaubitz, *eMagRes* **2018**, *7*, 79–92.
[53] E. Ravera, B. Corzilius, V. K. Michaelis, C. Rosa, R. G. Griffin, C. Luchinat, Bertini, *J. Am. Chem. Soc.* **2013**, *135*, 1641–1644.
[54] R. Ghosh, Y. Xiao, J. Kragelj, K. K. Frederick, *J. Am. Chem. Soc.* **2021**, *143*, 18454–18466.
[55] D. J. Hirsh, G. W. Brudvig, *Nat. Protoc.* **2007**, *2*, 1770–1781.

Manuscript received: August 12, 2024
Accepted manuscript online: November 14, 2024
Version of record online: November 28, 2024